Electronic Supplementary Material

Mesoscale Study of Crystal Plane Effects of Ni Catalysts on CO_2 Hydrogenation

Xiaolei Wang[1], Ning Liu[2], Ruinian Xu[2], Biaohua Chen[2,*], Chengna Dai[2], Gangqiang Yu[2]

1 College of Life Sciences and Chemistry, Jiangsu Second Normal University, Nanjing 210013, China

2 College of Environment and Energy Engineering, Beijing University of Technology, Beijing 100124, China

*. *Corresponding author:* Biaohua Chen

Email: chenbh@bjut.edu.cn

Contents

Fig. S14. Reaction potential energy diagrams via formate route: (a) Ni(111), (b) Ni(322), (c) Ni(100) and (d) Ni(110).

Fig. S15. Reaction potential energy diagrams via CO_2 direct dissociate + CO hydrogenation route: (a) Ni(111), (b) Ni(322), (c) Ni(100) and (d) Ni(110).

Fig. S16. Reaction potential energy diagrams via carboxyl route: (a) Ni(111), (b) Ni(322), (c) Ni(100) and (d) Ni(110).

Fig. S17. Reaction potential energy diagrams via C hydrogenation route: (a) Ni(111), (b) Ni(322), (c) Ni(100) and (d) Ni(110).

Fig. S18. Calculated steady-state reaction rates of step R3, R14 and step R20 over (a) Ni(111), (b) Ni(322), (c) Ni(100) and (d) Ni(110) facets.

Fig. S19. Potential energy diagram of optimal pathway for the formation of CH_4 and CO on Ni(111) and Ni(100) facets.

Fig. S20. Calculated reaction rates of CH_4 and CO formation over (a) Ni(111), (b) Ni(322), (c) Ni(100) and (d) Ni(110) facets.

Fig. S21. Comparison of CH_4 selectivity simulated by microkinetic model and experimental results.

Table S1 Elementary reaction steps and rate equations of CO_2 hydrogenation reaction.

Table S2 Preferred adsorption sites and adsorption energies of all intermediates in CO_2 hydrogenation reaction on Ni(111), Ni(322), Ni(100) and Ni(110) surfaces.

Table S3 Reactions energies (E_a) and active barriers (ΔE) in CO_2 hydrogenation reaction on Ni(111), Ni(322), Ni(100) and Ni(110) surfaces.

Table S4 Reaction rate (s^{-1}) of CH_4 and CO formation at different temperatures.

Table S5 Comparison of experimental and calculated reaction rate (s^{-1}) of CH_4 and CO formation.

S1. Detailed equations of CO_2 conversion and CH_4 selectivity

After gas chromatography, it was found that the gas phase products were CH_4 and CO, and the liquid was H_2O. The correction factors for carbon monoxide and methane relative to argon were 1.04 and 2.15, respectively. The CO_2 conversion (X_A) and CH_4 selectivity (S_i) were calculated as

$$X_A = \frac{n_A^0 - n_A}{n_A^0} \times 100\% = \frac{A_A^0 / A_s^0 - A_A / A_s}{A_A^0 / A_s^0} \times 100\% \qquad (S1)$$

$$S_i = \frac{A_i \times F_{i/s}}{A_i \times F_{i/s} + A_j \times F_{j/s}} \times 100\% \qquad (S2)$$

where A_A^0 / A_s^0 was the peak area ratio of CO_2 and internal standard Ar in the reaction raw material gas, and A_A / A_s was the peak area ratio of CO_2 and internal standard Ar in the mixed gas after the reaction. A_i and A_j represented the peak areas of CO and CH_4, respectively, and $F_{i/s}$ and $F_{j/s}$ represented the relative correction factors of CO and CH_4, respectively.

The turnover frequency (TOF) was evaluated using 0.02-0.1 g catalyst, and the gas velocity was adjusted to keep the CO_2 conversion rate below 20%.

$$TOF(s^{-1}) = \frac{X_{\mathrm{CO_2}} \times F_{\mathrm{CO_2}}}{m_{cat} \times M_s} \qquad (S3)$$

F_{CO2} represented the flow rate of carbon dioxide in the feed gas (s^{-1}), and M_s was the number of active sites per unit mass of the catalyst. The active sites were measured via CO chemisorption, assuming that one CO molecule was adsorbed on one single Ni site.[1-3]

The activation energies of CO_2 conversion or CH_4 generation were calculated from the slope of Arrhenius plot 'lnTOF~1000/T' in Fig. S6. Compared with the Arrhenius equation below, the activation energy Ea ($kJ \cdot mol^{-1}$) should be the slop of Arrhenius plot multiplied by *R*.

$$\ln TOF = \ln A - \frac{E_a}{RT} \qquad (S4)$$

In which *A* presented the pre-exponential factor, *Ea* meant the activation energy and R meant the gas constant R (8.314 $J \cdot (mol \cdot K)^{-1}$).

S2. Calculation method of reaction rate for elementary reaction

The forward / reverse pre-exponential factors (ν_{for} and ν_{rev}) for reaction X+Y→Z were determined as

$$\nu_{for} = \prod_{i=1}^{3N} \nu_i^{IS} / \prod_{j=1}^{3N-1} \nu_j^{TS} \tag{S5}$$

$$\nu_{rev} = \prod_{i=1}^{3N} \nu_i^{FS} / \prod_{j=1}^{3N-1} \nu_j^{TS} \tag{S6}$$

where ν_i^{IS} and ν_i^{FS} were vibrational frequencies at initial and final state, and ν_j^{TS} was vibrational frequencies at transition state[4].

Thus the rate constant (k_n) was calculated as

$$k_n = \nu \exp(\text{-}E_a / k_B T) \tag{S7}$$

where E_a was the activation energy barrier and k_B was Boltzmann constant.

For the adsorption process, the rates would be written as[5]

$$k_{ads}^i = s_0 P_i A_i / \sqrt{2\pi m_i k_B T} \tag{S8}$$

where s_0, P_i (Pa) and m_i (kg) were the sticking coefficient, partial pressure and molecular mass of species I, respectively; A_i (m^2) was the area of adsorption site.

For the desorption process, the rates were calculated based on the harmonic transition state theory (HTST) and it could be derived as Arrhenius equation[6, 7]:

$$k_{des} = \frac{k_B T}{h} e^{n_1} \left(\frac{P^\Theta}{RT}\right)^{1-n} \exp\left(\frac{\Delta_r S_m^\Theta \left(P^\Theta\right)}{R}\right) \exp\left(\frac{-E_a}{RT}\right) \tag{S9}$$

$$\Delta_r S_m^\Theta \left(P^\Theta\right) = S_{TS}^\Theta \left(P^\Theta\right) - S_{RS}^\Theta \left(P^\Theta\right) \tag{S10}$$

where n and n_1 represented the coefficient amount of the reactants and the coefficient amount of the gaseous reactants. For the condensed phase reaction, the value of n_1 was 1. h and R were Plank constant and gas constant, respectively. The entropy $\Delta_r S_m^\Theta \left(P^\Theta\right)$ contained three contributions, translational, rotational, and vibrational distributions, which was obtained from the frequency calculations with DFT at 1 atm and 298.15 K.

S3. Microkinetic modeling

As shown in Fig. S7 and Table S1, the reaction network was divided into 31 elementary reaction steps. Here in, according to the actual experimental condition, the partial pressure of H_2 and CO_2 ($p1$ and $p2$) were set to be 60,000 Pa and 15,000 Pa, respectively. The reaction rates of elementary reactions have been expressed by ki, pi and y(i), and the parameters y(i) would obtained by solving 22 equations below. Therefore the steady state reaction rate of each elementary step and the intermediate surface coverage ratios could be calculated by the MATLAB program.

y(i)	Represented coverage	y(i)	Represented coverage
y(1)	θ_{*}	y(12)	θ_{HCOH*}
y(2)	θ_{H*}	y(13)	θ_{CH_2*}
y(3)	θ_{CO_2*}	y(14)	θ_{CO*}
y(4)	θ_{HCOO*}	y(15)	θ_{O*}
y(5)	θ_{H_2COO*}	y(16)	θ_{C*}
y(6)	θ_{H_2COOH*}	y(17)	θ_{CH*}
y(7)	θ_{H_2CO*}	y(18)	θ_{COOH*}
y(8)	θ_{OH*}	y(19)	θ_{COH*}
y(9)	θ_{HCOOH*}	y(20)	θ_{COHOH*}
y(10)	θ_{HCO*}	y(21)	θ_{CH_3*}
y(11)	θ_{H_2COH*}	y(22)	θ_{H_2O*}

Reaction rate equations in MATLAB program:

```
r1 = k1p1*y(1)^2 - k_1*y(2)^2;
r2 = k2p2*y(1) - k_2*y(3);
r3 = k3*y(3)*y(2) - k_3*y(4)*y(1);
r4 = k4*y(4)*y(2) - k_4*y(5)*y(1);
r5 = k5*y(5)*y(2) - k_5*y(6)*y(1);
```

r6 = k6*y(6)*y(1) - k_6*y(7)*y(8);

r7 = k7*y(4)*y(2) - k_7*y(9)*y(1);

r8 = k8*y(9)*y(1) - k_8*y(10)*y(8);

r9 = k9*y(10)*y(2) - k_9*y(7)*y(1);

r10 = k10*y(7)*y(2) - k_10*y(11)*y(1);

r11 = k11*y(10)*y(2) - k_11*y(12)*y(1);

r12 = k12*y(2)*y(12) - k_12*y(11)*y(1);

r13 = k13*y(11)*y(1) - k_13*y(13)*y(8);

r14 = k14*y(3)*y(1) - k_14*y(14)*y(15);

r15 = k15*y(14)*y(2) - k_15*y(10)*y(1);

r16 = k16*y(14)*y(1) - k_16*y(16)*y(15);

r17 = k17*y(16)*y(2) - k_17*y(17)*y(1);

r18 = k18*y(17)*y(2) - k_18*y(13)*y(1);

r19 = k19*y(12)*y(1) - k_19*y(17)*y(8);

r20 = k20*y(3)*y(2) - k_20*y(18)*y(1);

r21 = k21*y(18)*y(1) - k_21*y(14)*y(8);

r22 = k22*y(14)*y(2) - k_22*y(19)*y(1);

r23 = k23*y(18)*y(2) - k_23*y(20)*y(1);

r24 = k24*y(20)*y(1) - k_24*y(19)*y(8);

r25 = k25*y(19)*y(2) - k_25*y(12)*y(1);

r26 = k26*y(13)*y(2) - k_26*y(21)*y(1);

r27 = k27*y(21)*y(2);

r28 = k28*y(15)*y(2) - k_28*y(8)*y(1);

r29 = k29*y(8)*y(2) - k_29*y(22)*y(1);

r30 = k30*y(22);

r31 = k31*y(14);

Equations to be solved in MATLAB program:

dy(2) = 2*r1 - r3 - r4 - r5 - r7 - r9 - r10 - r11 - r12 - r15 - r17 - r18 - r20 - r22 - r23 - r25 - r26- r27 - r28 - r29;

```
dy(3) = r2 - r3 - r14 - r20;
dy(4) = r3 - r4 - r7;
dy(5) = r4 - r5;
dy(6) = r5 - r6;
dy(7) = r6 + r9 - r10;
dy(8) = r6 + r8 + r13 + r19 + r21 + r24 + r28 - r29;
dy(9) = r7 - r8;
dy(10) = r8 - r9 - r11 + r15;
dy(11) = r10 + r12 - r13;
dy(12) = r11 - r12 - r19 + r25;
dy(13) = r13 + r18 - r26;
dy(14) = r14 - r15 - r16 + r21 - r22 -r31;
dy(15) = r14 + r16 - r28;
dy(16) = r16 - r17;
dy(17) = r17 - r18 + r19;
dy(18) = r20 - r21 - r23;
dy(19) = r22 + r24 - r25;
dy(20) = r23 - r24;
dy(21) = r26 - r27;
dy(22) = r29 - r30;
dy(1) = - dy(2) - dy(3) - dy(4) - dy(5) - dy(6) - dy(7) - dy(8) - dy(9) - dy(10) - dy(11) -
dy(12) - dy(13) - dy(14) - dy(15) - dy(16) - dy(17) - dy(18) - dy(19) - dy(20) - dy(21) -
dy(22);
```

S4. Theoretical CH_4 selectivity

The theoretical selectivity of CH_4 was obtained by equation S11:

$$S_{\mathrm{CH_4}} = \frac{r_{\mathrm{CH_4}}}{r_{\mathrm{CH_4}} + r_{\mathrm{CO}}} \times 100\% \tag{S11}$$

$S_{\mathrm{CH_4}}$ was the selectivity of CH_4, $r_{\mathrm{CH_4}}$ and r_{CO} represented the generation rate of CH_4

and CO, respectively.

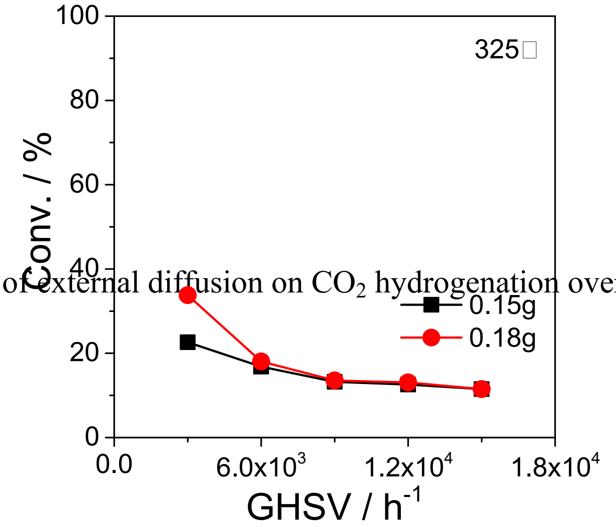

Fig. S1. Influence of external diffusion on CO_2 hydrogenation over Ni-BN at 325 °C.

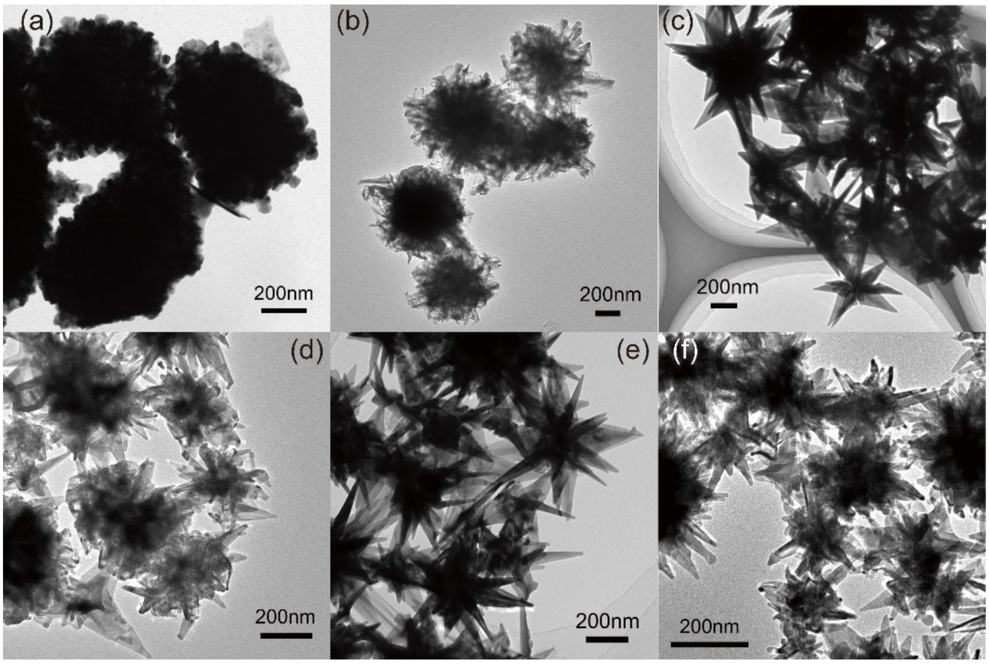

Fig. S2. Morphologies of Ni synthesized under same temperature of 150 °C and time of 3 h but various H_2 pressure: (a) 0 bar, (b) 1 bar, (c) 6 bar, (d) 10 bar, (e) 14 bar, (f) 20 bar.

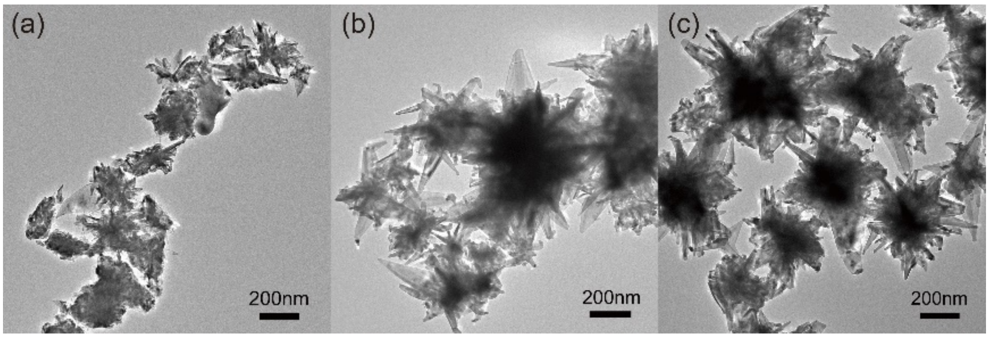

Fig. S3. Morphologies of 14 bar Ni synthesized under same temperature of 150 °C and various time: (a) 0.25 h, (b) 0.5 h, (c) 1 h.

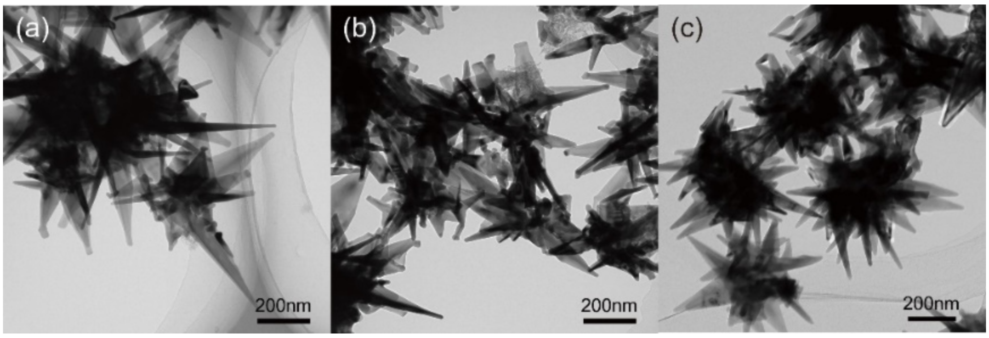

Fig. S4. Morphologies of 14 bar Ni synthesized under same time of 3h and various temperature: (a) 130 °C, (b) 150 °C, (c) 170 °C.

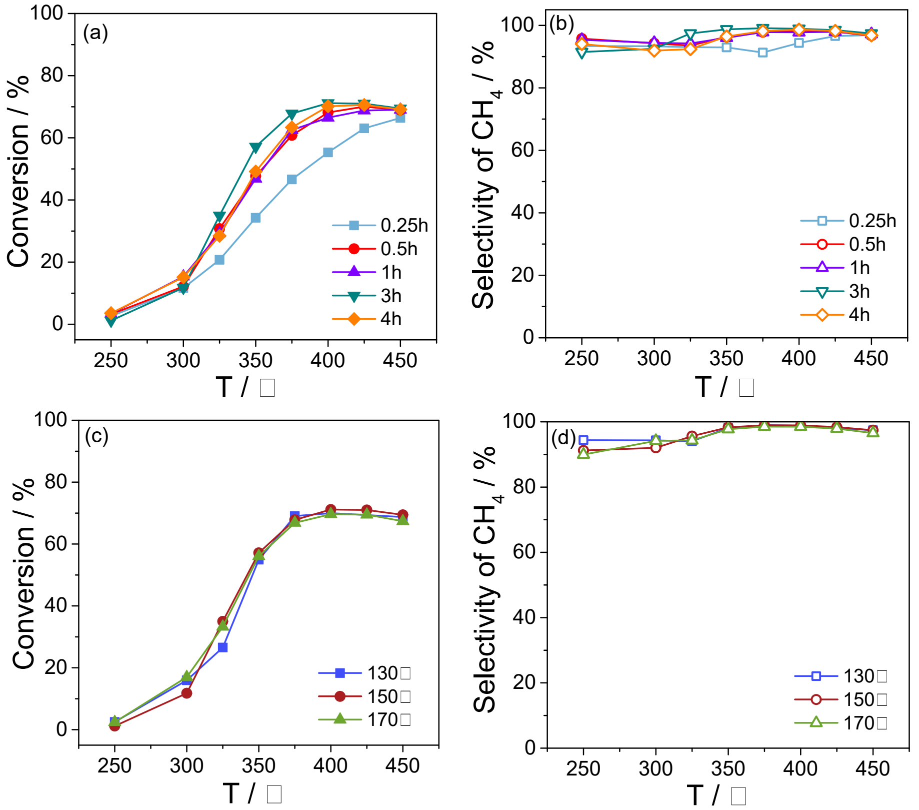

Fig. S5. Activity of CO_2 hydrogenation of Ni catalysts synthesized at (a, b) various synthesis time, (c, d) various synthesis temperature.

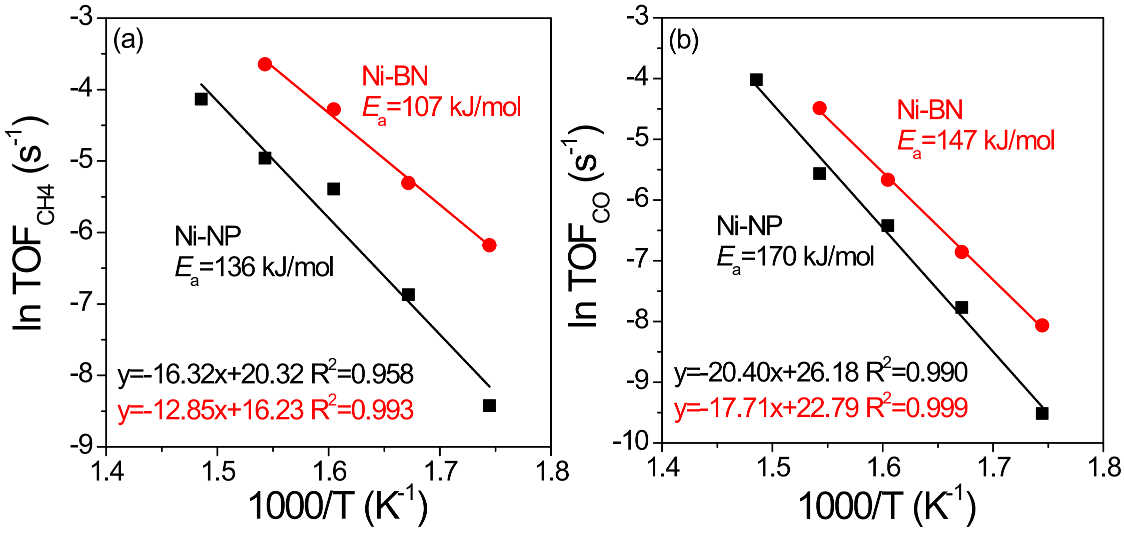

Fig. S6. Arrhenius plots of Ni-NP and Ni-BN: (a) CH_4, (b) CO.

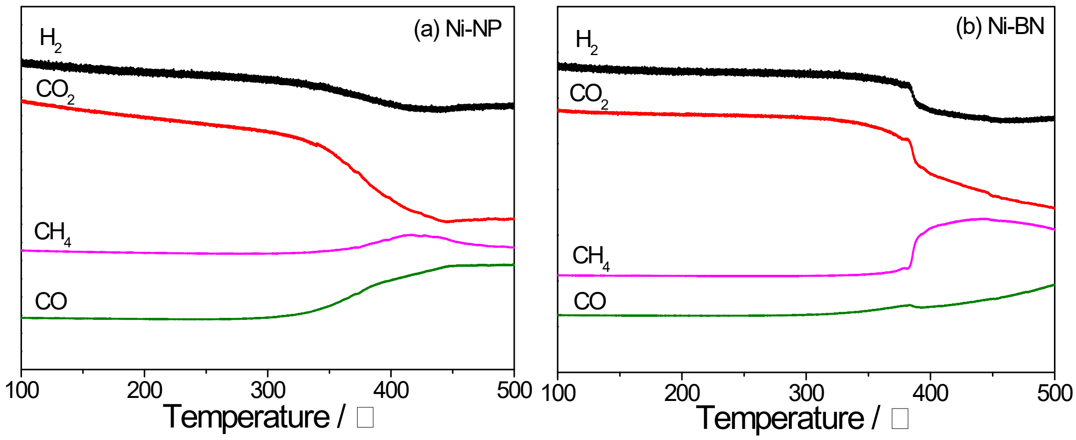

Fig. S7. TPSR-MS profiles for (a) Ni-NP and (b) Ni-BN catalysts.

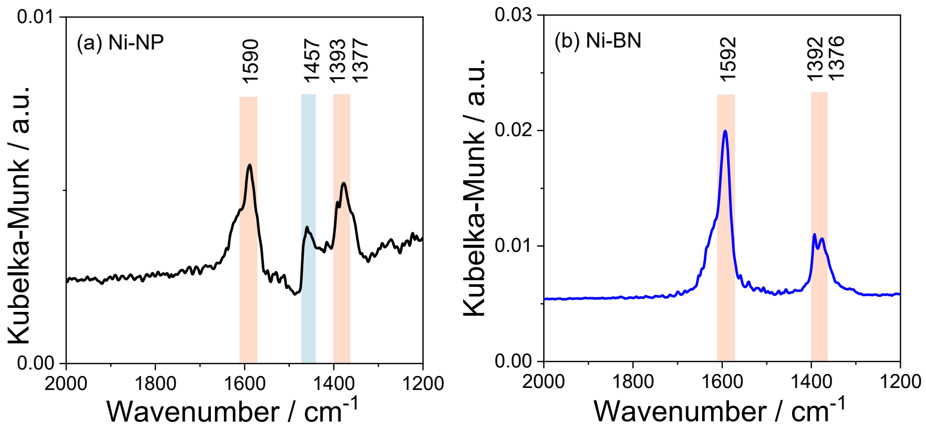

Fig. S8 In-situ DRIFTS results of CO_2 hydrogenation reaction on (a) Ni-NP and (b) Ni-BN catalyst being mixed with inter SiO_2 with CO_2 : H_2 = 1 : 4.

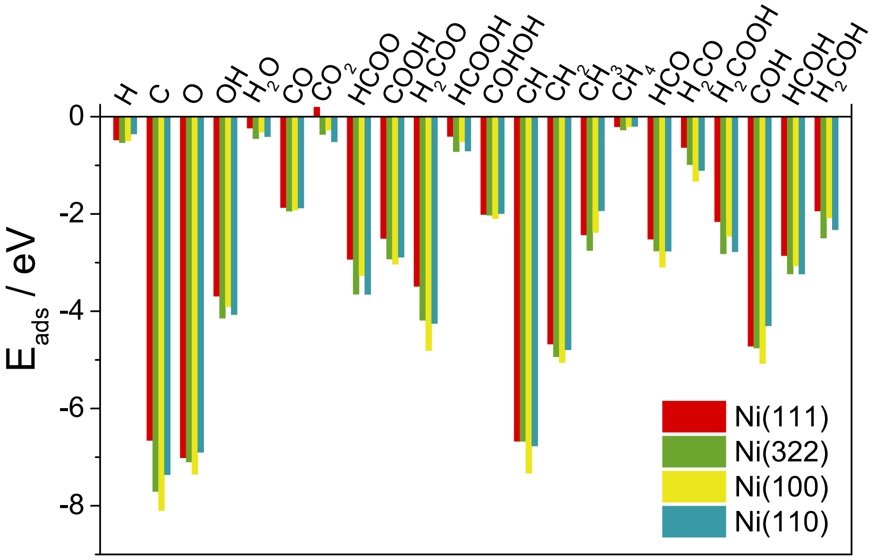

Fig. S9. Adsorption energies of all intermediates in CO_2 hydrogenation reaction on Ni(111), Ni(322), Ni(100) and Ni(110) surfaces.

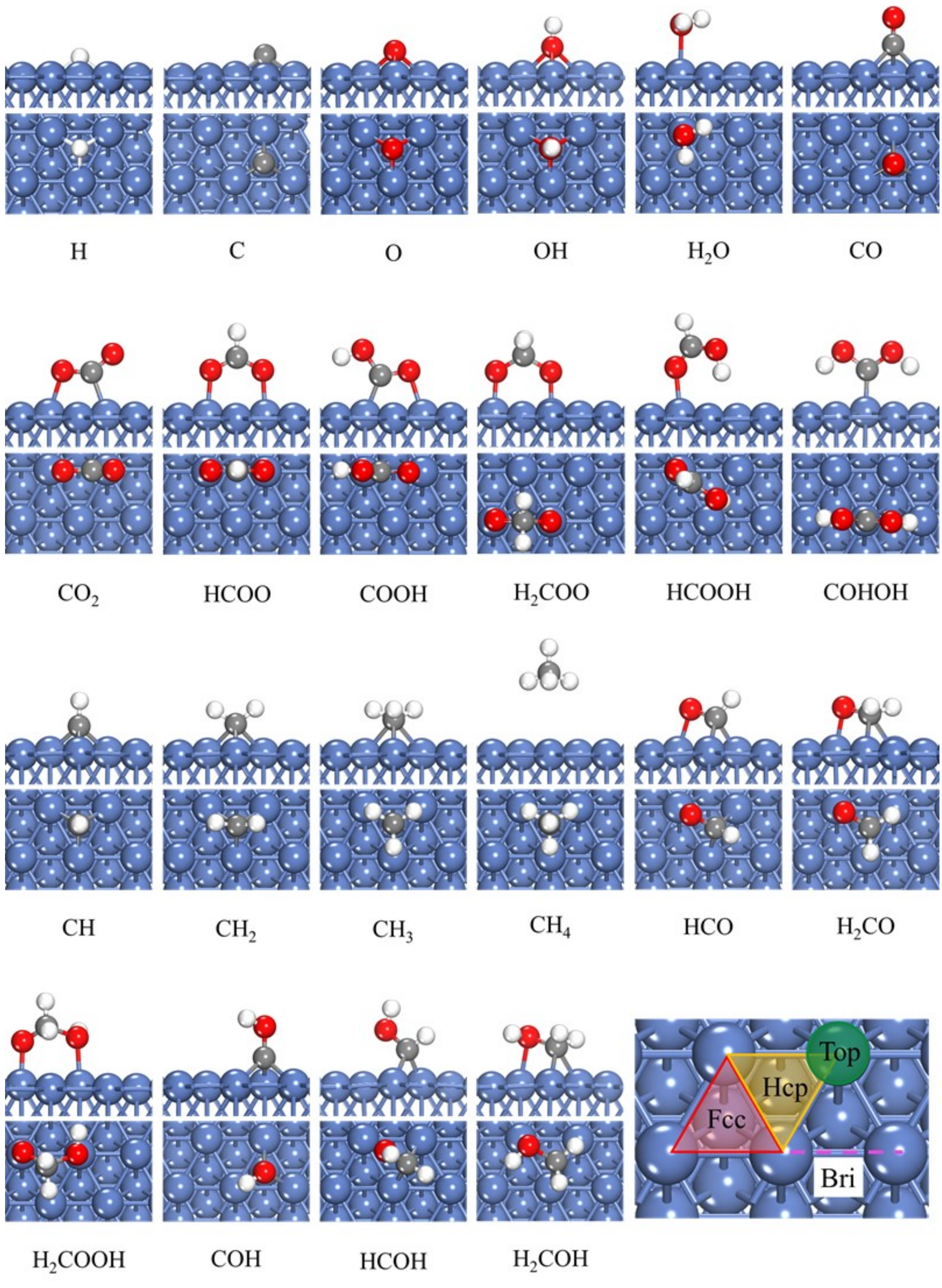

Fig. S10. Top and side view of the preferred adsorption sites of all intermediates in CO_2 hydrogenation on Ni(111) surface.

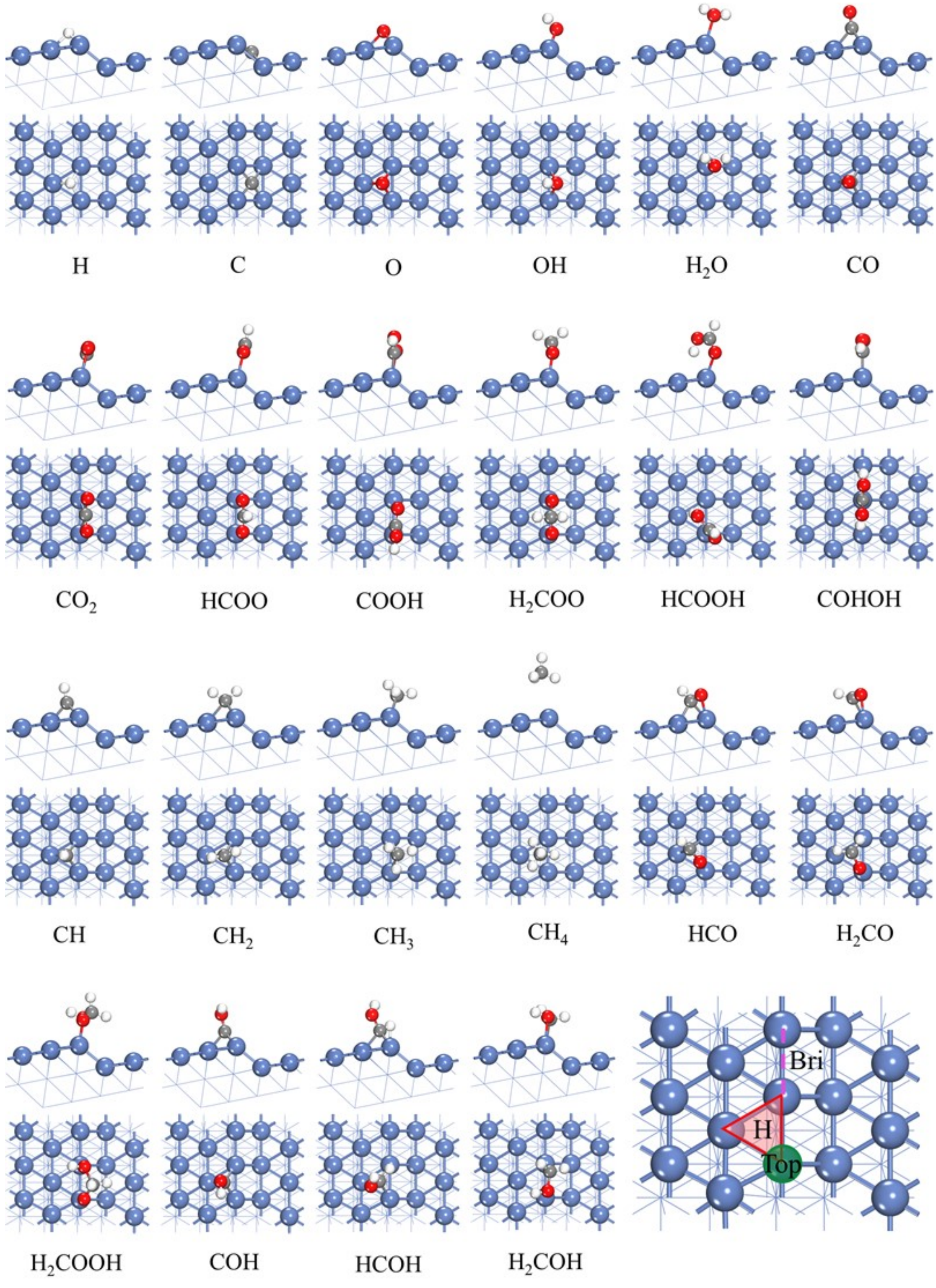

Fig. S11. Top and side view of the preferred adsorption sites of all intermediates in CO_2 hydrogenation on Ni(322) surface.

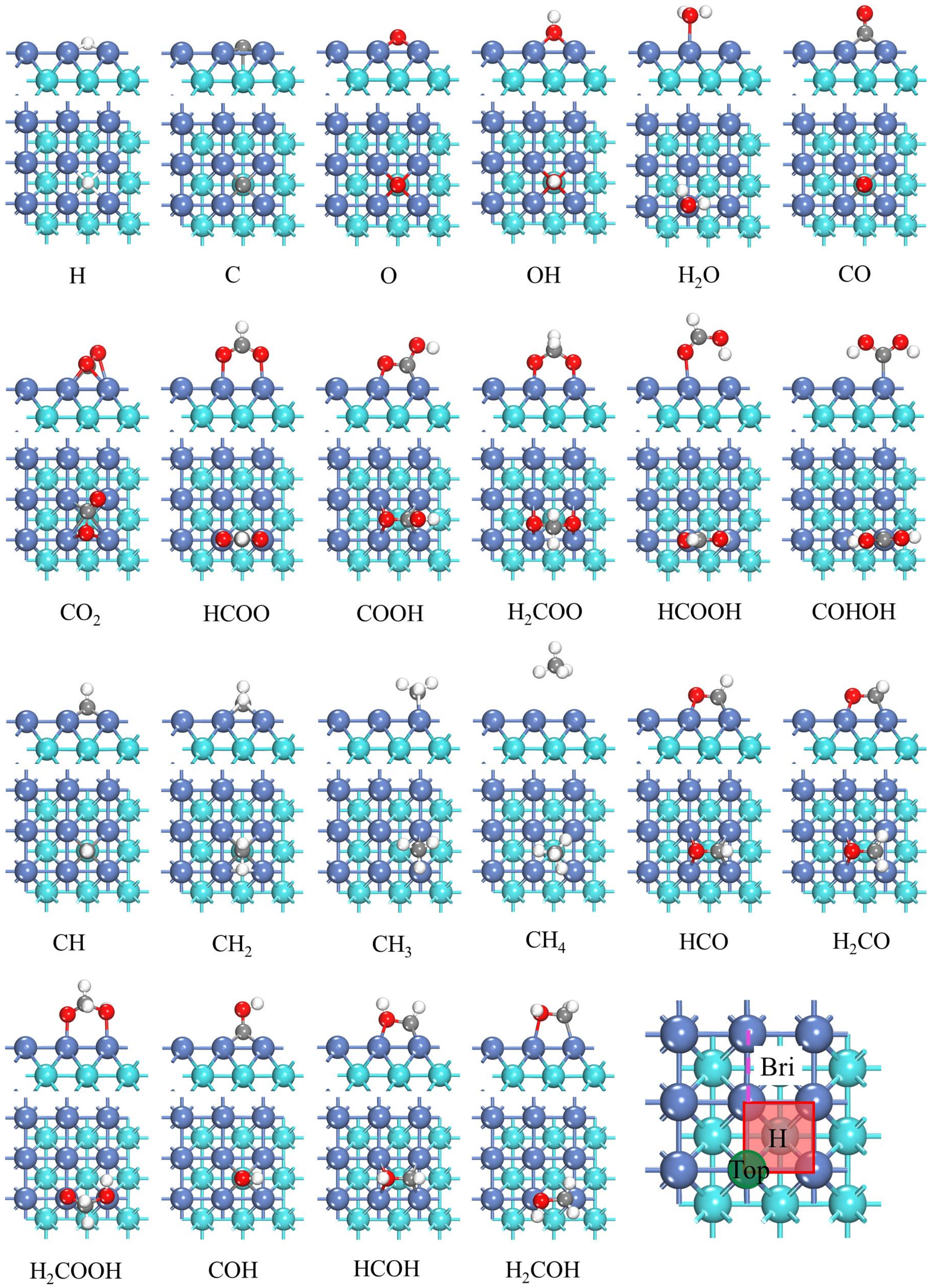

Fig. S12. Top and side view of the preferred adsorption sites of all intermediates in CO_2 hydrogenation on Ni(100) surface.

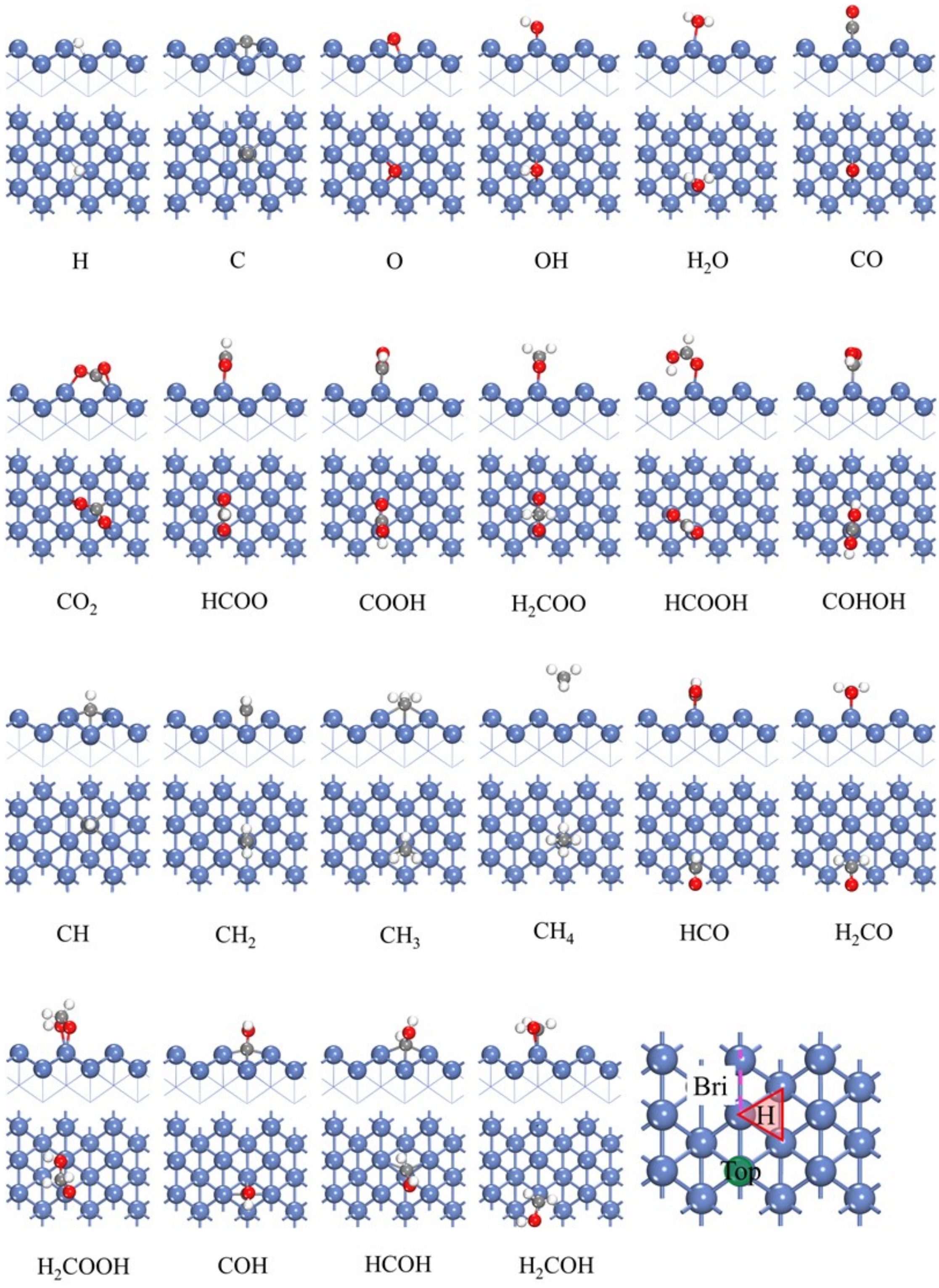

Fig. S13. Top and side view of the preferred adsorption sites of all intermediates in CO_2 hydrogenation on Ni(110) surface.

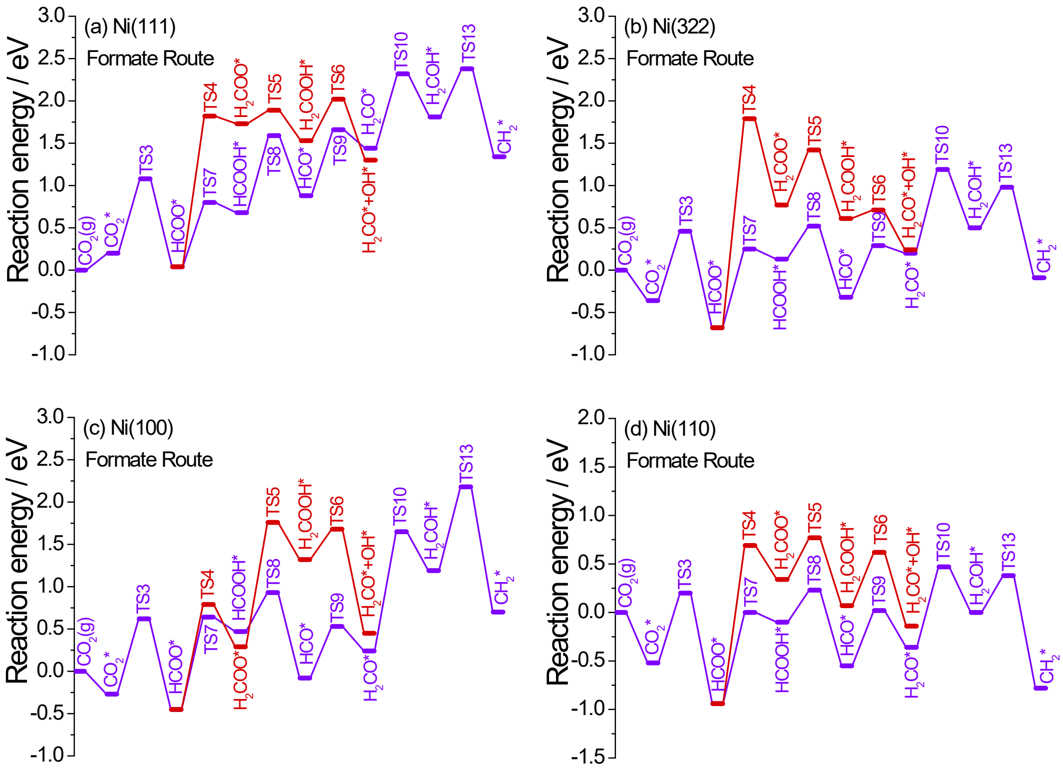

Fig. S14. Reaction potential energy diagrams via formate route: (a) Ni(111), (b) Ni(322), (c) Ni(100) and (d) Ni(110).

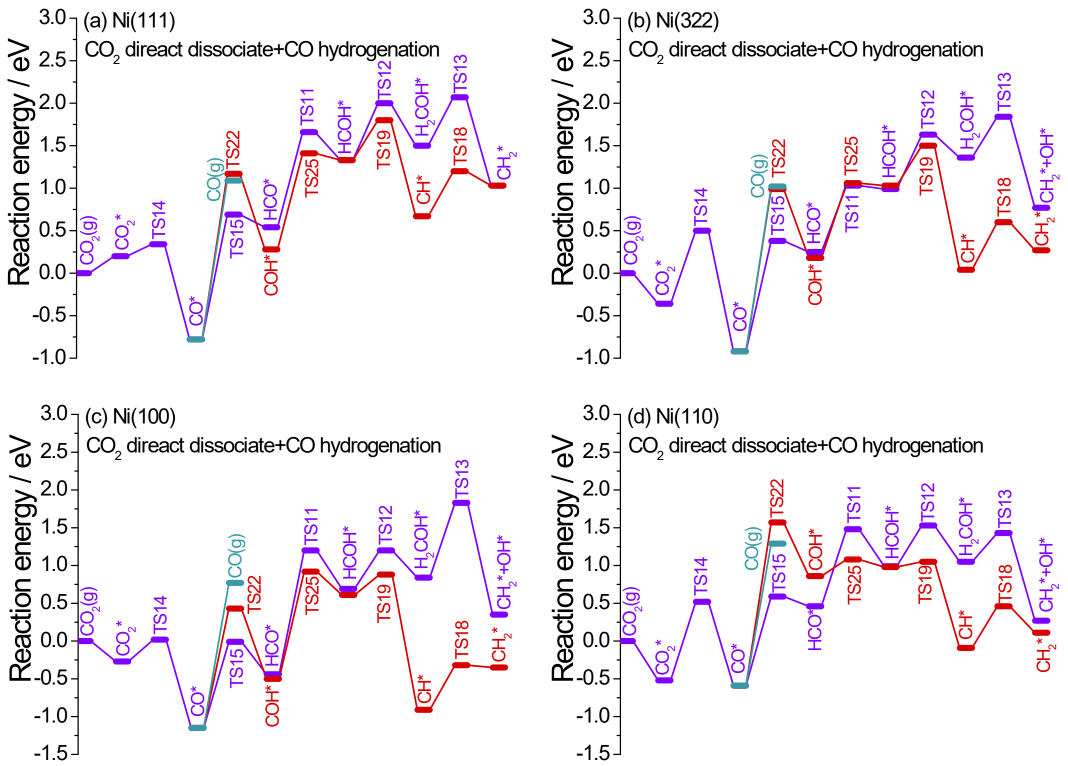

Fig. S15. Reaction potential energy diagrams via CO_2 direct dissociate + CO hydrogenation route: (a) Ni(111), (b) Ni(322), (c) Ni(100) and (d) Ni(110).

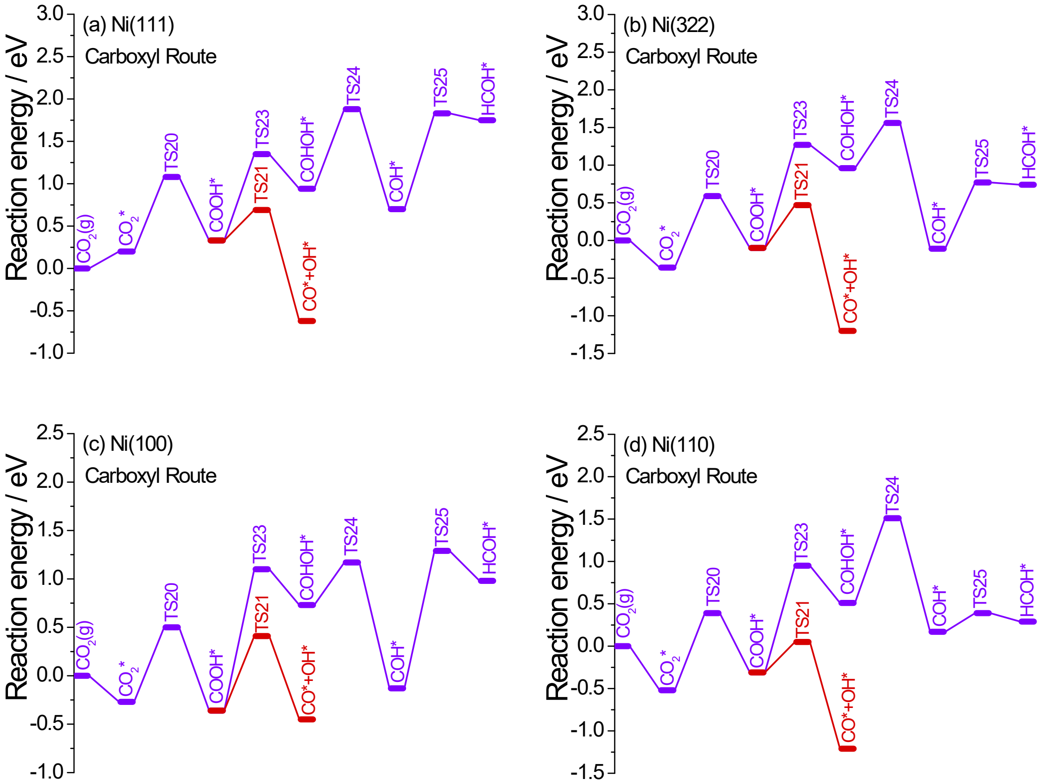

Fig. S16. Reaction potential energy diagrams via carboxyl route: (a) Ni(111), (b) Ni(322), (c) Ni(100) and (d) Ni(110).

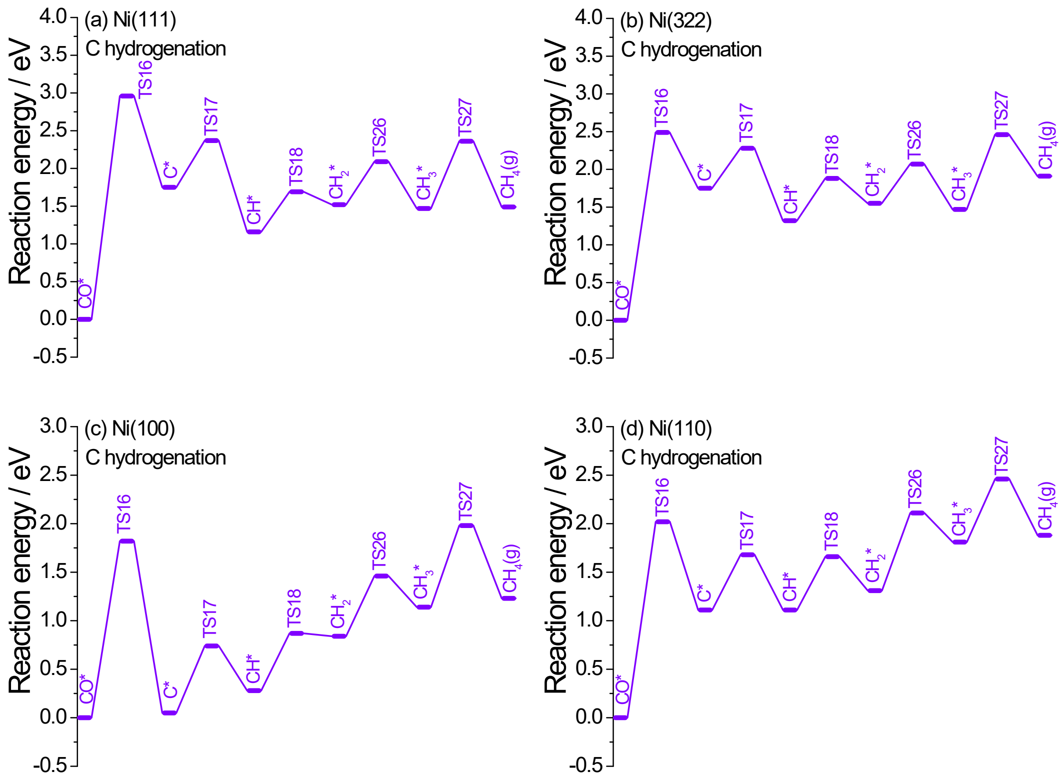

Fig. S17. Reaction potential energy diagrams via C hydrogenation route: (a) Ni(111), (b) Ni(322), (c) Ni(100) and (d) Ni(110).

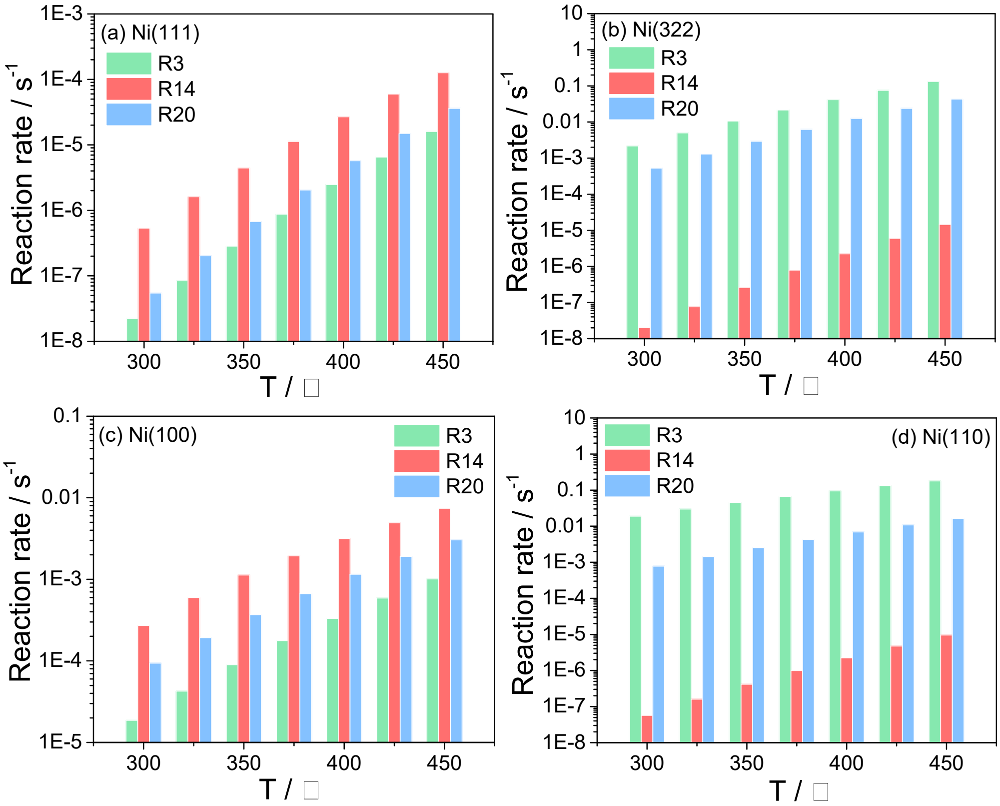

Fig. S18. Calculated steady-state reaction rates of step R3, R14 and step R20 over (a) Ni(111), (b) Ni(322), (c) Ni(100) and (d) Ni(110) facets.

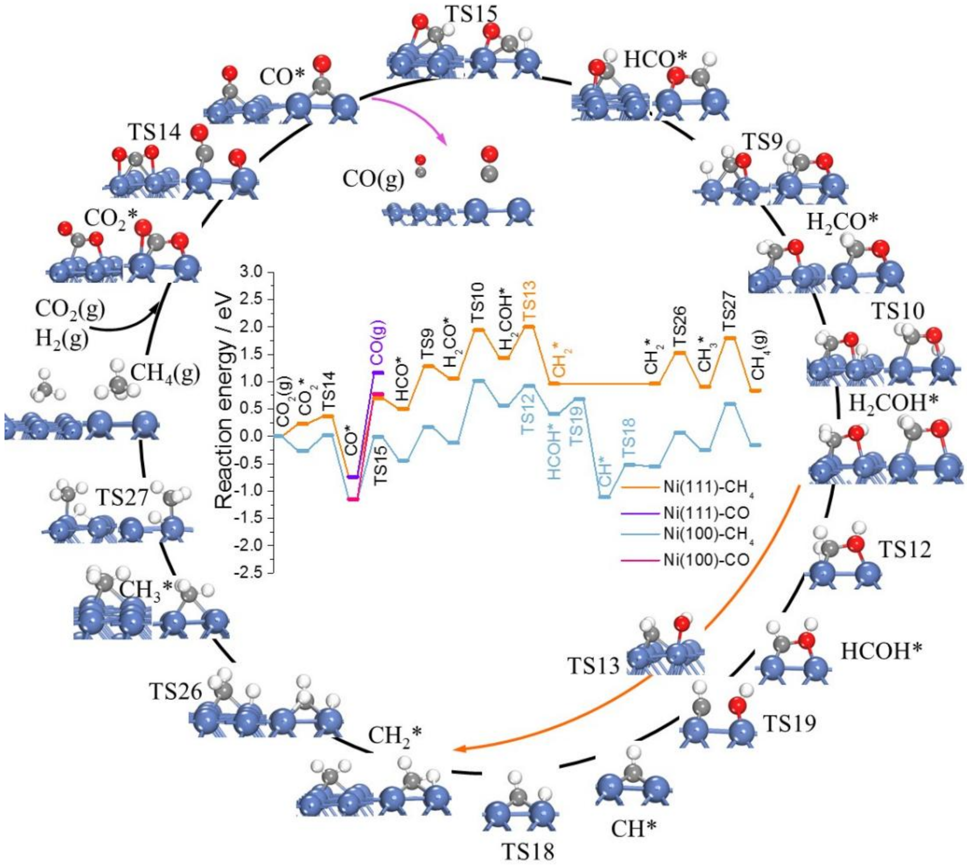

Fig. S19. Potential energy diagram of optimal pathway for the formation of CH_4 and CO on Ni(111) and Ni(100) facets.

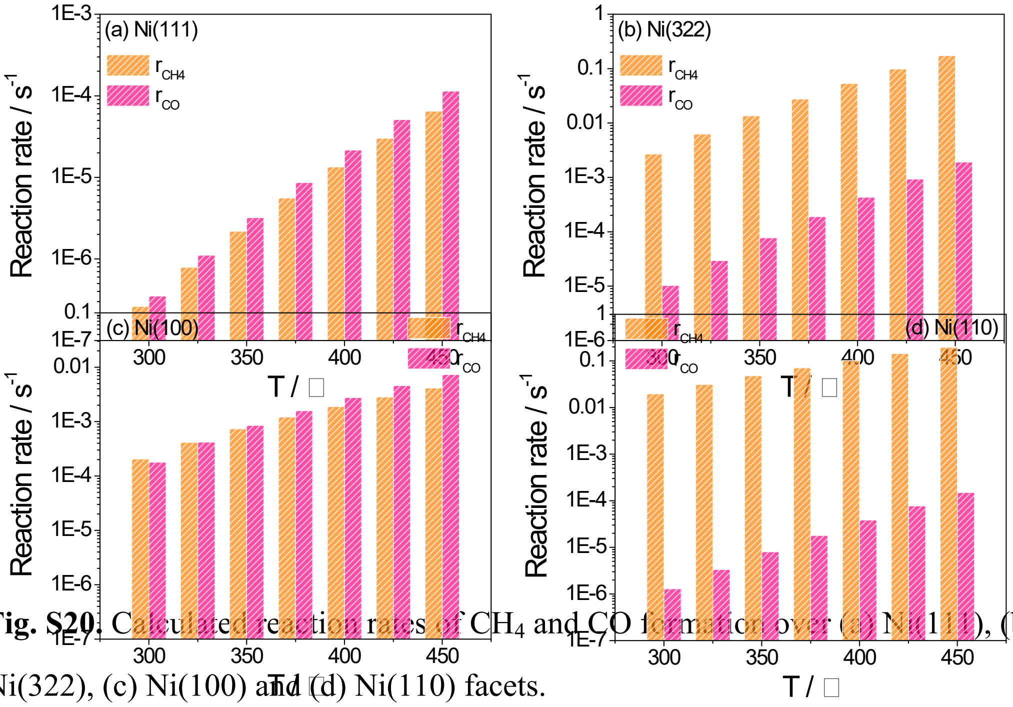

Fig. S20. Calculated reaction rates of CH_4 and CO formation over (a) Ni(111), (b) Ni(322), (c) Ni(100) and (d) Ni(110) facets.

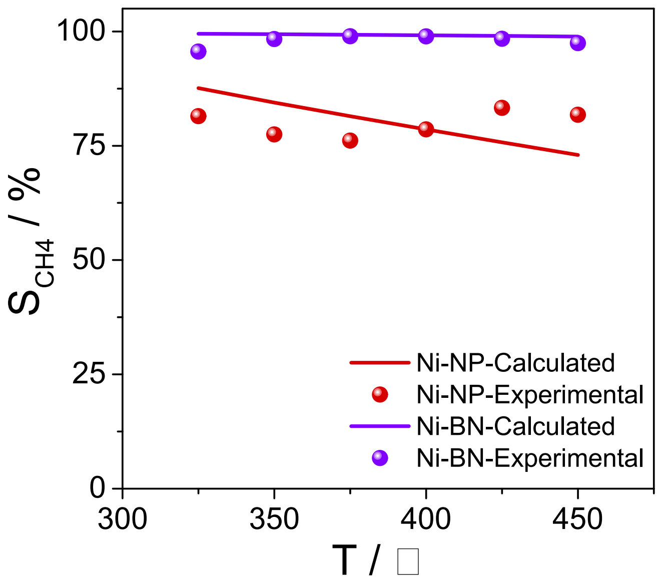

Fig. S21. Comparison of CH_4 selectivity simulated by microkinetic model and experimental results.

Table S1 Elementary reaction steps and rate equations of CO_2 hydrogenation reaction.

No.	Elementary reaction steps	Reaction rate equations
R1	$H_2(g)+2^* \leftrightarrow 2H^*$	$r_1=k_1P_{H_2}\theta_*^2-k_{-1}\theta_{H^*}^2$
R2	$CO_2(g)+^* \leftrightarrow CO_2{}^*$	$r_2=k_2P_{CO_2}\theta_*-k_{-2}\theta_{CO_2{}^*}$
R3	$CO_2{}^*+H^* \leftrightarrow HCOO^*+^*$	$r_3=k_3\theta_{CO_2{}^*}\theta_{H^*}-k_{-3}\theta_{HCOO^*}\theta_*$
R4	$HCOO^*+H^* \leftrightarrow H_2COO^*+^*$	$r_4=k_4\theta_{HCOO^*}\theta_{H^*}-k_{-4}\theta_{H_2COO^*}\theta_*$
R5	$H_2COO^*+H^* \leftrightarrow H_2COOH^*+^*$	$r_5=k_5\theta_{H_2COO^*}\theta_{H^*}-k_{-5}\theta_{H_2COOH^*}\theta_*$
R6	$H_2COOH^*+^* \leftrightarrow H_2CO^*+OH^*$	$r_6=k_6\theta_{H_2COOH^*}\theta_*-k_{-6}\theta_{H_2CO^*}\theta_{OH^*}$
R7	$HCOO^*+H^* \leftrightarrow HCOOH^*+^*$	$r_7=k_7\theta_{HCOO^*}\theta_{H^*}-k_{-7}\theta_{HCOOH^*}\theta_*$
R8	$HCOOH^*+^* \leftrightarrow HCO^*+OH^*$	$r_8=k_8\theta_{HCOOH^*}\theta_*-k_{-8}\theta_{HCO^*}\theta_{OH^*}$
R9	$HCO^*+H^* \leftrightarrow H_2CO^*+^*$	$r_9=k_9\theta_{HCO^*}\theta_{H^*}-k_{-9}\theta_{H_2CO^*}\theta_*$
R10	$H_2CO^*+H^* \leftrightarrow H_2COH^*+^*$	$r_{10}=k_{10}\theta_{H_2CO^*}\theta_{H^*}-k_{-10}\theta_{H_2COH^*}\theta_*$
R11	$HCO^*+H^* \leftrightarrow HCOH^*+^*$	$r_{11}=k_{11}\theta_{HCO^*}\theta_{H^*}-k_{-11}\theta_{HCOH^*}\theta_*$
R12	$HCOH^*+H^* \leftrightarrow H_2COH^*+^*$	$r_{12}=k_{12}\theta_{HCOH^*}\theta_{H^*}-k_{-12}\theta_{H_2COH^*}\theta_*$
R13	$H_2COH^*+^* \leftrightarrow CH_2{}^*+OH^*$	$r_{13}=k_{13}\theta_{H_2COH^*}\theta_*-k_{-13}\theta_{CH_2{}^*}\theta_{OH^*}$
R14	$CO_2{}^*+^* \leftrightarrow CO^*+O^*$	$r_{14}=k_{14}\theta_{CO_2{}^*}\theta_*-k_{-14}\theta_{CO^*}\theta_{O^*}$
R15	$CO^*+^* \leftrightarrow HCO^*+^*$	$r_{15}=k_{15}\theta_{CO^*}\theta_{H^*}-k_{-15}\theta_{HCO^*}\theta_*$
R16	$CO^*+^* \leftrightarrow C^*+O^*$	$r_{16}=k_{16}\theta_{CO^*}\theta_*-k_{-16}\theta_{C^*}\theta_{O^*}$
R17	$C^*+H^* \leftrightarrow CH^*+^*$	$r_{17}=k_{17}\theta_{C^*}\theta_{H^*}-k_{-17}\theta_{CH^*}\theta_*$
R18	$CH^*+H^* \leftrightarrow CH_2{}^*+^*$	$r_{18}=k_{18}\theta_{CH^*}\theta_{H^*}-k_{-18}\theta_{CH_2{}^*}\theta_*$
R19	$HCOH^*+^* \leftrightarrow CH^*+OH^*$	$r_{19}=k_{19}\theta_{HCOH^*}\theta_*-k_{-19}\theta_{CH^*}\theta_{OH^*}$
R20	$CO_2{}^*+H^* \leftrightarrow COOH^*+^*$	$r_{20}=k_{20}\theta_{CO_2{}^*}\theta_{H^*}-k_{-20}\theta_{COOH^*}\theta_*$
R21	$COOH^*+^* \leftrightarrow CO^*+OH^*$	$r_{21}=k_{21}\theta_{COOH^*}\theta_*-k_{-21}\theta_{CO^*}\theta_{OH^*}$
R22	$CO^*+H^* \leftrightarrow COH^*+^*$	$r_{22}=k_{22}\theta_{CO^*}\theta_{H^*}-k_{-22}\theta_{COH^*}\theta_*$
R23	$COOH^*+H^* \leftrightarrow COHOH^*+^*$	$r_{23}=k_{23}\theta_{COOH^*}\theta_{H^*}-k_{-23}\theta_{COHOH^*}\theta_*$
R24	$COHOH^*+^* \leftrightarrow COH^*+OH^*$	$r_{24}=k_{24}\theta_{COHOH^*}\theta_*-k_{-24}\theta_{COH^*}\theta_{OH^*}$
R25	$COH^*+H^* \leftrightarrow HCOH^*+^*$	$r_{25}=k_{25}\theta_{COH^*}\theta_{H^*}-k_{-25}\theta_{HCOH^*}\theta_*$
R26	$CH_2{}^*+H^* \leftrightarrow CH_3{}^*+^*$	$r_{26}=k_{26}\theta_{CH_2{}^*}\theta_{H^*}-k_{-26}\theta_{CH_3{}^*}\theta_*$
R27	$CH_3{}^*+H^* \rightarrow CH_4(g)+2^*$	$r_{27}=k_{27}\theta_{CH_3{}^*}\theta_{H^*}$
R28	$O^*+H^* \leftrightarrow OH^*+^*$	$r_{28}=k_{28}\theta_{O^*}\theta_{H^*}-k_{-28}\theta_{OH^*}\theta_*$
R29	$OH^*+H^* \leftrightarrow H_2O^*+^*$	$r_{29}=k_{29}\theta_{OH^*}\theta_{H^*}-k_{-29}\theta_{H_2O^*}\theta_*$
R30	$H_2O^* \rightarrow H_2O(g)+^*$	$r_{30}=k_{30}\theta_{H_2O^*}$
R31	$CO^* \rightarrow CO(g)+^*$	$r_{31}=k_{31}\theta_{CO^*}$

Table S2 Preferred adsorption sites and adsorption energies of all intermediates in CO_2 hydrogenation reaction on Ni(111), Ni(322), Ni(100) and Ni(110) surfaces.

Intermediates	Ni(111)		Ni(322)		Ni(100)		Ni(110)	
	Site	E_{ads}^{ZPE}	Site	E_{ads}^{ZPE}	Site	E_{ads}^{ZPE}	Site	E_{ads}^{ZPE}
H	Fcc	-0.48	H	-0.53	Bri	-0.50	H	-0.35
C	Hcp	-6.66	H	-7.71	H	-8.10	H	-7.36
O	Fcc	-7.01	H	-7.10	H	-7.35	H	-6.90
OH	Fcc	-3.69	Bri	-4.14	H	-3.91	Bri	-4.07
H_2O	Top	-0.23	Top	-0.45	Top	-0.32	Top	-0.41
CO	Hcp	-1.87	H	-1.94	H	-1.92	Bri	-1.88
CO_2	Bri	0.20	Bri	-0.36	H	-0.27	H	-0.52
HCOO	Bri	-2.93	Bri	-3.65	Bri	-3.27	Bri	-3.65
COOH	Bri	-2.50	Bri	-2.93	H	-3.03	Bri	-2.89
H_2COO	Bri	-3.49	Bri	-4.19	H	-4.81	Bri	-4.25
HCOOH	Top	-0.40	Bri	-0.72	Bri	-0.51	Top	-0.71
COHOH	Top	-2.01	Bri	-2.03	Bri	-2.10	Bri	-1.99
CH	Fcc	-6.67	H	-6.67	H	-7.33	H	-6.77
CH_2	Fcc	-4.68	H	-4.94	H	-5.06	H	-4.79
CH_3	Fcc	-2.43	Bri	-2.75	Bri	-2.38	H	-1.93
CH_4	Fcc	-0.21	H	-0.27	H	-0.21	H	-0.20
HCO	Fcc	-2.52	H	-2.76	H	-3.09	Bri	-2.77
H_2CO	Fcc	-0.63	H	-0.99	H	-1.33	Bri	-1.11
H_2COOH	Bri	-2.16	Bri	-2.82	Bri	-2.46	Top	-2.78
COH	Hcp	-4.72	H	-4.76	H	-5.08	H	-4.30
HCOH	Bri	-2.86	H	-3.23	H	-3.07	H	-3.23
H_2COH	Fcc	-1.94	Top	-2.49	Bri	-2.08	Bri	-2.32

Table S3 Reactions energies (E_a) and active barriers (ΔE) in CO_2 hydrogenation reaction on Ni(111), Ni(322), Ni(100) and Ni(110) surfaces.

Reaction	Ni(111)		Ni(322)		Ni(100)		Ni(110)	
	E_a	ΔE	E_a	ΔE	E_a	ΔE	E_a	ΔE
R1	0.0	-0.96	0.0	-1.06	0.0	-1.00	0.0	-0.70
R2	0.0	0.20	0.0	-0.36	0.0	-0.27	0.0	-0.52
R3	0.88	-0.15	0.82	-0.32	0.89	-0.18	0.72	-0.41
R4	1.78	1.69	2.47	1.46	1.24	0.74	1.63	1.28
R5	0.16	-0.20	0.65	-0.16	1.47	1.03	0.43	-0.27
R6	0.49	-0.22	0.10	-0.37	0.36	-0.87	0.55	-0.22
R7	0.76	0.65	0.93	0.81	1.09	0.92	0.94	0.84
R8	0.91	0.21	0.39	-0.45	0.46	-0.54	0.33	-0.45
R9	0.78	0.56	0.61	0.52	0.61	0.32	0.57	0.19
R10	0.88	0.37	0.99	0.31	1.41	0.96	0.83	0.36
R11	1.12	0.79	0.78	0.73	1.64	1.13	1.02	0.53
R12	0.67	0.18	0.64	0.37	0.51	0.14	0.54	0.06
R13	0.57	-0.47	0.48	-0.59	0.99	-0.49	0.38	-0.78
R14	0.14	-0.99	0.86	-0.56	0.29	-0.87	1.04	-0.07
R15	1.47	1.33	1.30	1.17	1.14	0.71	1.18	1.06
R16	2.96	1.76	2.49	1.75	1.82	0.05	2.02	1.11
R17	0.62	-0.59	0.53	-0.43	0.69	0.22	0.57	0.00
R18	0.53	0.36	0.56	0.23	0.59	0.55	0.55	0.20
R19	0.47	-0.66	0.47	-0.99	0.27	-1.52	0.07	-1.07
R20	0.88	0.13	0.95	0.26	0.77	-0.09	0.91	0.21
R21	0.36	-0.95	0.57	-1.10	0.61	-0.69	0.36	-0.90
R22	1.95	1.06	1.91	1.10	1.58	0.65	2.16	1.45
R23	1.02	0.62	1.37	1.05	1.46	1.09	1.26	0.82
R24	0.94	-0.24	0.60	-1.07	0.44	-0.86	1.00	-0.34
R25	1.13	1.05	0.88	0.85	1.42	1.11	0.22	0.11
R26	0.57	-0.05	0.52	-0.08	0.62	0.30	0.80	0.51
R27	0.89	0.02	0.99	0.45	0.84	0.09	0.65	0.08
R28	1.05	0.17	0.98	-0.16	1.36	0.43	0.47	-0.43
R29	1.17	0.39	1.01	0.69	1.27	0.47	1.18	0.48
R30	0.23	0.0	0.45	0.0	0.32	0.0	0.41	0.0
R31	1.87	0.0	1.94	0.0	1.93	0.0	1.88	0.0

Table S4 Reaction rate (s^{-1}) of CH_4 and CO formation at different temperatures.

Temperature / °C		300	325	350	375	400	425	450
Ni(111)	r_{CH4} / s^{-1}	2.62E-7	7.89E-7	2.18E-6	5.59E-6	1.34E-5	3.02E-5	6.47E-5
	r_{CO} / s^{-1}	3.51E-7	1.11E-6	3.21E-6	8.63E-6	2.16E-5	5.10E-5	1.14E-4
Ni(322)	r_{CH4} / s^{-1}	2.69E-3	6.25E-3	1.35E-2	2.76E-2	5.34E-2	9.83E-2	1.73E-1
	r_{CO} / s^{-1}	1.03E-5	2.95E-5	7.74E-5	1.89E-4	4.31E-4	9.31E-4	1.91E-3
Ni(100)	r_{CH4} / s^{-1}	2.05E-4	4.15E-4	7.37E-4	1.21E-3	1.89E-3	2.84E-3	4.16E-3
	r_{CO} / s^{-1}	1.79E-4	4.18E-4	8.51E-4	1.58E-3	2.76E-3	4.58E-3	7.32E-3
Ni(110)	r_{CH4} / s^{-1}	1.97E-2	3.13E-2	4.79E-2	7.09E-2	1.02E-1	1.43E-1	1.96E-1
	r_{CO} / s^{-1}	1.29E-6	3.34E-6	8.01E-6	1.80E-5	3.84E-5	7.76E-5	1.50E-4
Ni-NP	r_{CH4} / s^{-1}	6.67E-4	1.09E-3	1.71E-3	2.57E-3	3.76E-3	5.36E-3	7.45E-3
	r_{CO} / s^{-1}	6.59E-5	1.54E-4	3.14E-4	5.86E-4	1.03E-3	1.71E-3	2.76E-3
Ni-BN	r_{CH4} / s^{-1}	2.66E-3	6.17E-3	1.34E-2	2.73E-2	5.27E-2	9.70E-2	1.71E-1
	r_{CO} / s^{-1}	1.13E-5	3.16E-5	8.16E-5	1.96E-4	4.42E-4	9.47E-4	1.93E-3

Table S5 Comparison of experimental and calculated reaction rate (s^{-1}) of CH_4 and CO formation.

	Temperature / °C		300	325	350	375	400	425	450
Exp.	Ni-NP	r_{CH4} / s^{-1}	2.19E-4	1.04E-3	4.55E-3	7.02E-3			
		r_{CO} / s^{-1}	7.36E-5	4.22E-4	1.63E-3	3.83E-3			
	Ni-BN	r_{CH4} / s^{-1}	2.07E-3	4.94E-3	1.39E-2	2.61E-2	1.60E-2		
		r_{CO} / s^{-1}	3.14E-4	1.05E-3	3.46E-3	1.13E-2	1.79E-2		
Miro.	Ni-NP	r_{CH4} / s^{-1}	6.67E-4	1.09E-3	1.71E-3	2.57E-3	3.76E-3	5.36E-3	7.45E-3
		r_{CO} / s^{-1}	6.59E-5	1.54E-4	3.14E-4	5.86E-4	1.03E-3	1.71E-3	2.76E-3
	Ni-BN	r_{CH4} / s^{-1}	2.66E-3	6.17E-3	1.34E-2	2.73E-2	5.27E-2	9.70E-2	1.71E-1
		r_{CO} / s^{-1}	1.13E-5	3.16E-5	8.16E-5	1.96E-4	4.42E-4	9.47E-4	1.93E-3
kMC	Ni(110)	r_{CH4} / s^{-1}	1.62E-4	2.77E-4	4.71E-4	7.15E-4	1.03E-3	1.48E-3	2.05E-3
	Ni-bn	r_{CH4} / s^{-1}	9.31E-3	1.66E-2	2.47E-2	3.40E-2	4.52E-2	5.27E-2	6.06E-2

Exp.: Experiment
Miro.: Mirokinetic modeling
kMC: kinetic Monte Carlo

References

[1] Italiano, C.;Llorca, J.;Pino, L.;Ferraro, M.;Antonucci, V.; Vita, A. CO and CO_2 methanation over Ni catalysts supported on CeO_2, Al_2O_3 and Y_2O_3 oxides. *Appl. Catal., B* **2020**, *264*, 118494.

[2] Jia, X.;Zhang, X.;Rui, N.;Hu, X.; Liu, C.-j. Structural effect of Ni/ZrO_2 catalyst on CO_2 methanation with enhanced activity. *Appl. Catal., B* **2019**, *244*, 159-169.

[3] Geyer, R.;Hunold, J.;Keck, M.;Kraak, P.;Pachulski, A.; Schödel, R. Methods for determining the metal crystallite size of Ni supported catalysts. *Chem. Ing. Tech.* **2012**, *84*, 160-164.

[4] Xu, L.;Mei, D.; Henkelman, G. Adaptive kinetic Monte Carlo simulation of methanol decomposition on Cu(100). *J. Chem. Phys.* **2009**, *131*, 244520.

[5] Cai, Q. X.;Wang, J. G.;Wang, Y. G.; Mei, D. Mechanistic insights into the structure-dependent selectivity of catalytic furfural conversion on platinum catalysts. *AIChE Journal* **2015**, *61*, 3812-3824.

[6] Piskorz, W.;Zasada, F.;Stelmachowski, P.;Diwald, O.;Kotarba, A.; Sojka, Z. Computational and experimental investigations into N_2O decomposition over MgO nanocrystals from thorough molecular mechanism to ab initio microkinetics. *J. Phys. Chem. C* **2011**, *115*, 22451-22460.

[7] Liu, N.;Zhang, R.;Chen, B.;Li, Y.; Li, Y. Comparative study on the direct decomposition of nitrous oxide over M (Fe, Co, Cu)–BEA zeolites. *J. Catal.* **2012**, *294*, 99-112.